nature communications

Article

https://doi.org/10.1038/s41467-024-50734-x

Multiple embryonic sources converge to form the pectoral girdle skeleton in zebrafish

Received: 27 July 2023

Accepted: 19 July 2024

Published online: 26 July 2024

Check for updates

Shunya Kuroda[1,3,4] ✉, Robert L. Lalonde[2,4], Thomas A. Mansour[1], Christian Mosimann[2] & Tetsuya Nakamura[1] ✉

The morphological transformation of the pectoral/shoulder girdle is fundamental to the water-to-land transition in vertebrate evolution. Although previous studies have resolved the embryonic origins of tetrapod shoulder girdles, those of fish pectoral girdles remain uncharacterized, creating a gap in the understanding of girdle transformation mechanisms from fish to tetrapods. Here, we identify the embryonic origins of the zebrafish pectoral girdle, including the cleithrum as an ancestral girdle element lost in extant tetrapods. Our combinatorial approach of photoconversion and genetic lineage tracing demonstrates that cleithrum development combines four adjoining embryonic populations. A comparison of these pectoral girdle progenitors with extinct and extant vertebrates highlights that cleithrum loss, indispensable for neck evolution, is associated with the disappearance of its unique developmental environment at the head/trunk interface. Overall, our study establishes an embryological framework for pectoral/shoulder girdle formation and provides evolutionary trajectories from their origin in water to diversification on land.

The pectoral girdle anchors the pectoral appendage (pectoral fin or forelimb) to the body wall in jawed vertebrates[1]. The pectoral girdle comprises of dermal bones and cartilage or their replacement bones (endoskeleton), while cartilaginous fishes secondarily lost the dermal components[2]. In bony vertebrates with paired fins living in water (sarcopterygians and actinopterygians), the cleithrum[3], one of the pectoral dermal bones, is both functionally and anatomically a major component. As vertebrates transitioned onto land, the relative size of the cleithrum in the pectoral girdle began to decrease and eventually disappeared independently in multiple lineages leading to extant tetrapods[1,4,5]. Consequently, except for some anuran amphibians[6,7] and possibly turtles[8], no extant tetrapods form the cleithrum, and enlarged endoskeletal elements are instead the dominant component of the pectoral girdle in tetrapods[9]. In contrast to these accumulating anatomical descriptions, the embryonic changes responsible for the evolutionary loss of the cleithrum and expansion of the endoskeleton remain elusive.

The major embryonic sources of the shoulder girdle in tetrapods have been identified by works in several model systems. Homotopic transplantations between chicken and quail embryos[10] and genetic cell lineage tracing using *Prx1:Cre* in mice[11] revealed that the clavicle, a dermal component of the shoulder girdle, derives mainly from the trunk lateral plate mesoderm (LPM). The same strategy of tissue transplantation and genetic cell lineage tracing using *Mef2c-AHF:Cre* mice (cardiopharyngeal marker) identified that the cardiopharyngeal mesoderm (CPM) also contributes to the medial extremity of the clavicle in chicken and mice[10,12]. The CPM or cardiopharyngeal field defines a deeply conserved progenitor field that forms at least in part within the anterior LPM[13–16]. Moreover, previous studies discovered that the scapula, an endoskeletal component of the girdle, in axolotls, chickens, and mice derives mainly from the trunk LPM and its dorsal portion from the somites, potentially due to the scapula's developmental position across these mesodermal boundaries[17–20].

[1]Department of Genetics, Rutgers the State University of New Jersey, Piscataway, NJ 08854, USA. [2]Department of Pediatrics, Section of Developmental Biology, University of Colorado School of Medicine, Anschutz Medical Campus, Aurora, CO, USA. [3]Present address: Institute for Frontier Science Initiative, Kanazawa University, Kakuma-machi, Kanazawa 920-1164, Japan. [4]These authors contributed equally: Shunya Kuroda, Robert L. Lalonde.
✉e-mail: kurodashunya@gmail.com; nakamura@dls.rutgers.edu

Consequently, the trunk LPM is an important contributor to both dermal and endoskeletal components in tetrapod shoulder girdles, while the CPM and somites contribute to their medial and dorsal margins to some extent.

Neural crest cells are migratory ectodermal cells with broad lineage potential that among its diverse descendant lineages contribute to canonical ectodermal tissues (neurons and gilia) and cranial mesenchymal tissues (skeletons and connective tissues)[21,22]. Previous work in axolotl tested the potential contribution of neural crest cells to the shoulder girdle, but did not detect any neural crest-derived cells in the shoulder girdle skeletons[23]. In contrast, tissue transplantations in chicken embryos[24] and genetic lineage tracing using *Sox10:Cre* mice (with *Sox10* being expressed in migratory neural crest cell[4]) identified that neural crest cells give rise to clavicles. More recent genetic tracing of *Wnt1:Cre* that marks pre-migratory neural crest cells in mice, however, found no neural crest cell-lineage in the shoulder girdle skeletons[11,12]. This inconsistency among lineage labeling studies may partially be due to the deployment of isolated *cis*-regulatory elements of different neural crest genes. The distribution of genetically labeled neural crest cell lineages in mice arguably varies depending on the *cis*-regulatory elements that drive Cre expression[25]. Consequently, the contribution of the neural crest cells to the shoulder skeletons must be resolved by additional cell lineage tracking such as region-specific photoconversions or tissue transplantations (see an example in ref. 26). Nonetheless, in sum, the contribution of neural crest cells to the tetrapod shoulder girdle has not been unambiguously determined and, if any, appears to be minor[4,24].

Revealing the developmental processes forming the pectoral girdle in actinopterygians would provide mechanistic insights into how such intricate tetrapod shoulder development was established. However, in contrast to the accumulated, yet incomplete knowledge of the embryonic origins of tetrapod shoulder girdles, less is known about the developmental lineages contributing to the pectoral girdles of fishes with paired fins. Previous work assumed that the embryonic origin of the dermal pectoral components, including the fish cleithrum, is the neural crest, but this assumption has not yet been tested[4]. In contrast, *Sox10:Cre*-labeled lineages did not contribute to dermal components of the pectoral girdle in zebrafish[27]. However, this could be partially due to the deployment of *Sox10* regulatory elements from mice in the used transgenics that might not fully recapitulate zebrafish *sox10* expression or lineage. The endoskeletal scapulocoracoid, a cartilaginous precursor for the scapula and coracoid, seems to be formed within the fin bud mesenchyme in the larval zebrafish (reviewed in ref. 28), yet the embryonic origins of the endoskeletal component have not been fully identified either. Accordingly, the embryonic origins of the dermal and endoskeletal pectoral girdle components in bony fishes remain to be determined.

In zebrafish, the cleithrum lies between the head and trunk structures in the absence of a forming neck in fishes (Fig. 1a); the cleithrum posteriorly delineates the most caudal pharyngeal arch and the pericardium, the mesothelium-lined body cavity encapsulating the heart (Fig. 1b, c), and anteriorly delineates the trunk lateral body wall where the pectoral fin attaches (Fig. 1b, c). Moreover, the cleithrum develops closely associated with the pectoral musculature: cleithrohyoid, pectoral fin adductor/abductor, and posterior hypaxial muscles (Fig. 1b, c, see Supplementary Note 1 for nomenclature summary). Embryologically, these anatomical components associated with the cleithrum derive from distinct embryonic sources:

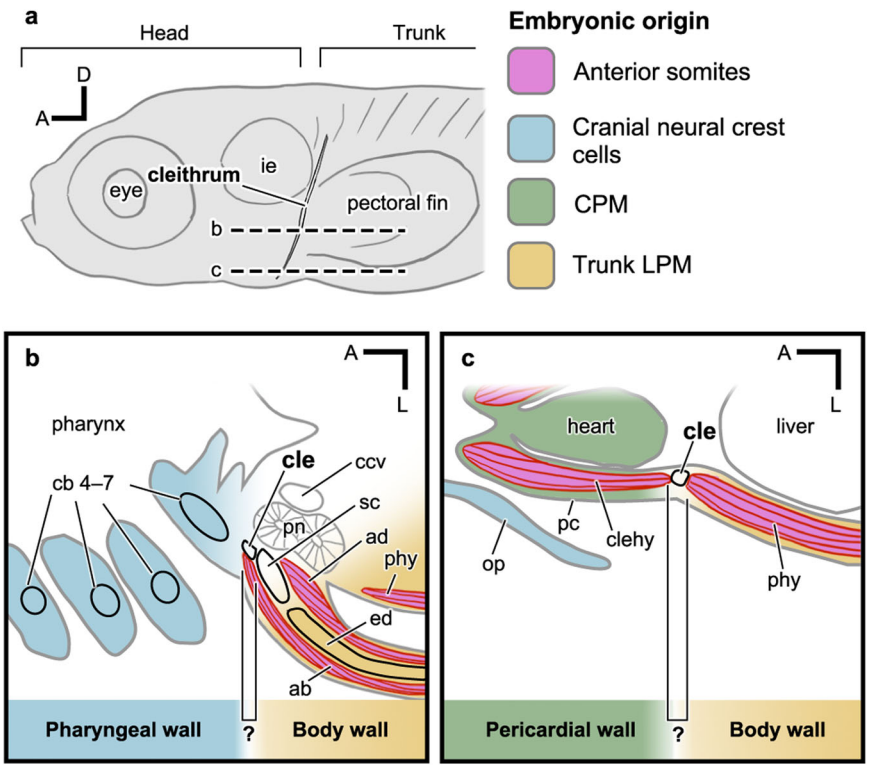

Fig. 1 | The anatomical position and developmental environment of the pectoral girdle. a Left lateral view of the larval zebrafish. **b**, **c** Schematic view of horizontal sections obtained from two dorsoventrally different levels as indicated in (**a**), showing that the larval cleithrum is located at the interface made by multiple embryonic populations: anterior somites (pink), cranial neural crest cells (light blue), CPM (green), and trunk LPM (yellow). The embryonic origins of the pectoral girdle that develops at the boundary of fin-field LPM, cranial neural crest cells, and CPM remains to be identified. **b**, **c** Were drawn after open data sets available on Zebromes (https://neurodata.io/project/zebromes/) originally published in ref. 95. A anterior, ab abductor muscle, ad adductor muscle, cb 4–7 ceratobranchial 4–7, ccv common cardinal vein, cle cleithrum, clehy cleithrohyoid muscle, CPM cardiopharyngeal mesoderm, D dorsal, ed endoskeletal disc, ie inner ear, LPM lateral plate mesoderm, op operculum, pc pericardium, phy posterior hypaxial muscle, pn pronephros, sc scapulocoracoid.

https://doi.org/10.1038/s41467-024-50734-x

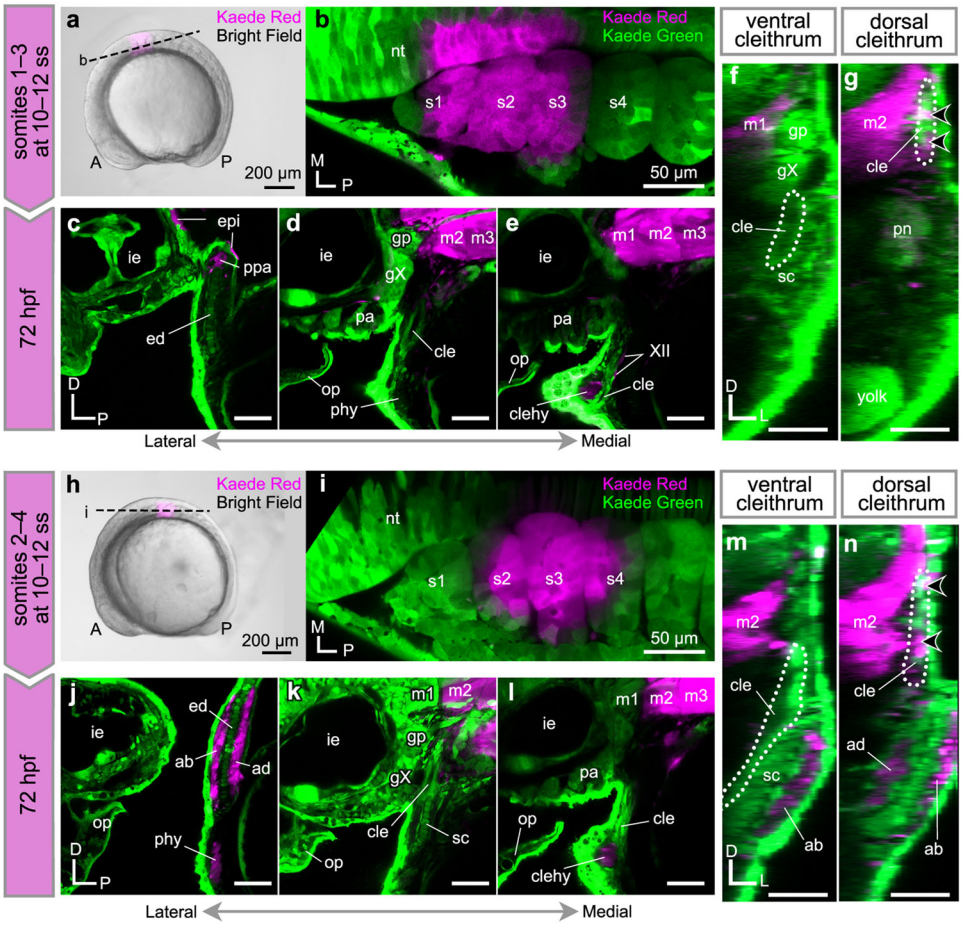

Fig. 2 | Contribution of anterior somites to pectoral muscles and dorsal cleithrum. a, **b** Photoconversion of the anterior three somites and adjacent neural tube at the 10–12 somite stage (ss), viewed from the left lateral side (**a**) and in horizontal confocal section (**b**) ($n = 10$). Kaede-red is pseudo-colored in magenta. **c**–**e** Confocal parasagittal sections of 72 hpf embryos from lateral (**c**) to medial (**e**) show that labeled cells are in the anterior three myotomes and cleithrohyoid muscle, but not in the ventral cleithrum ($n = 8/8$). **f**, **g** Transverse confocal sections obtained at the level of ventral (**f**) and dorsal (**g**) cleithrum found that labeled cells are in the dorsal cleithrum in a mosaic manner (arrowheads, $n = 4/8$), but not in ventral cleithrum. **h**, **i** Photoconversion of the somites 2–4 at the 10–12 ss ($n = 14/14$). **j**–**l** At 72 hpf, parasagittal confocal sections obtained from the medial (**j**) to lateral (**l**) levels show that labeled cells are in the adductor and abductor fin muscles ($n = 10/14$), posterior hypaxial muscles ($n = 10/14$), myotomes ($n = 13/14$), and cleithrohyoid muscle ($n = 10/14$), but not in the ventral cleithrum ($n = 14/14$). **m**, **n** Transverse confocal sections obtained at the level of ventral (**m**) and dorsal (**n**) cleithrum show that labeled cells are found in the dorsal cleithrum (arrowheads, $n = 4/14$), but not in ventral cleithrum.XII, hypoglossal nerve; A anterior, ab abductor muscle, ad adductor muscle, cle cleithrum, clehy cleithrohyoid muscle, ed endoskeletal disc, epi epidermis, gp posterior lateral line ganglion, gX vagus ganglia, i inner ear, op operculum, P posterior, pa pharyngeal arches, phy posterior hypaxial muscle, ppa primary pectoral artery, sc scapulocoracoid, m1–3 myotomes 1–3, nt neural tube, pn pronephros, s1–4 somites 1–4. Scale bars: (**a** and **h**) 200 µm, (**b**–**g**, **i**–**n**) 50 µm.

the pharyngeal arch mesenchyme from cranial neural crest cells[27,29], the pericardium from the LPM including *tbx1*-expressing CPM[30,31], the lateral body wall (mesothelium and connective tissues of the posterior hypaxial muscle) and pectoral fin bud from the trunk LPM[31–33], and the pectoral musculature from anterior somites[34,35]. Thus, given its anatomically unique position, cleithrum development in zebrafish potentially deploys any of these diverse embryonic cell populations (Fig. 1a–c).

Here, by combining region-specific photoconversions and genetic cell lineage analyses, we labeled the anterior somites, cranial neural crest cells, CPM, and trunk LPM to identify the embryonic lineage contributions to the pectoral girdle skeleton in zebrafish. Our results document that the cleithrum develops as a mosaic bone from multiple embryonic populations, while the scapulocoracoid exclusively derives from the fin field-associated LPM. A broad evolutionary comparison of the topographical position of the cleithrum implies that the multiple embryonic origins of the pectoral girdle skeletons are shared features among extinct and extant cleithrum-bearing species. Our data further propose that the evolutionary loss of the cleithrum in amniotes might have followed rearrangements of the ancestral developmental environment at the origins of the neck.

Results

Anterior somites give rise to pectoral musculature and the dorsal cleithrum

Previous work found that somites 1–4 are the major contributors to the pectoral musculature in zebrafish[35]. Of these, mesenchymal cells derived from somites 1-3 ventrally migrate over the prospective cleithrum area between the pharynx and the pectoral fin bud (Fig. 1a–c) and eventually develop into the cleithrohyoid muscle at the bottom of the pharynx[33,35]. We therefore tested whether these somitic mesenchymal cells also contribute to the cleithrum along their migratory route. To this end, we injected Kaede mRNA, encoding a photoconvertible protein, into one-cell stage embryos[36] (see Methods for details) and labeled somites 1–3 by Kaede photoconversion from green to red fluorescence (Kaede-red) at the 10–12 somite stage (mid-segmentation period[37]) (Fig. 2a, b). We then examined the contribution of labeled cells to the pectoral region at 72 h post-fertilization (hpf) (protruding

mouth stage[37]) when the bone matrix of the cleithrum, cartilage, and skeletal muscles become histologically and molecularly evident (see Supplementary Fig. 1). Due to laser illumination (405 nm) through the outside of the embryos to target somites, areas of the epidermis and neural tube dorsally and medially adjacent to the target somites, respectively, were also labeled (Fig. 2b). Given the lack of their contribution to skeletogenic mesenchyme[38], these non-mesodermal cells were not expected to affect the analysis of somite-derived cell lineages (Fig. 2c). Labeled cells derived from the anterior three somites were found in the first to third myotomes (Fig. 2d, e) and the cleithrohyoid muscle (Fig. 2e, $n = 8/8$). The observed contributions of the anterior three somites to the myotomes and the cleithrohyoid muscle are consistent with previous reports[34,35], supporting the efficacy of our photoconversion. Kaede-red signal was not found in the ventral cleithrum cells ($n = 0/8$; cleithrum positive/all labeled embryos), but in the cells delineating the dorsal cleithrum at the level of the myotome 2 ($n = 4/8$) (Fig. 2d–g; Supplementary Data 1). To comprehensively investigate the contribution of the anterior somites, we also photoconverted somites 2–4 at the 10–12 somite stage (Fig. 2h, i). At 72 hpf, labeled cells were found in the pectoral fin adductor/abductor muscles, posterior hypaxial muscles, myotomes 2–4, and cleithrohyoid muscle (Fig. 2j–l). These distributions also align with previous reports[34,35]. Again, cells labeled with Kaede-red were not found in the ventral cleithrum ($n = 0/14$) or scapulocoracoid ($n = 0/14$), but were distributed in the dorsal cleithrum ($n = 4/14$) (Fig. 2k–n; Supplementary Data 1).

To genetically trace the somitic lineages in the pectoral region, we analyzed *tbx6:cre; ubi:Switch* embryos that switch the reporter expression from EGFP to mCherry upon Cre expression driven by the *tbx6* paraxial mesoderm promoter (Supplementary Fig. 2a–g)[38,39]. At 72 hpf embryos, labeled cells were found in the anterior myotomes, adductor and abductor pectoral muscles, posterior hypaxial muscles, and cleithrohyoid muscles (Supplementary Fig. 2a–d). The *tbx6:cre* lineage cells were also sparsely distributed in the scapulocoracoid (Supplementary Fig. 2c) and ventral cleithrum (Supplementary Fig. 2e), and densely in the dorsal cleithrum (Supplementary Fig. 2f). The sparse labeled cells in the scapulocoracoid and ventral cleithrum could be a consequence of an additional labeling of the LPM lineage at the gastrulation stage, when *tbx6* expression does not explicitly discern the LPM and paraxial mesoderm[39]. We confirmed that the labeled cells in the dorsal cleithrum were osteoblasts by colocalization of mCherry and *sp7* expression (Supplementary Fig. 2g), supporting the somitic contributions to dorsal cleithrum osteoblasts. Since the labeled dorsal cleithrum cells were exclusively at the level of the paraxial mesoderm dorsoventrally, these cells seem to derive from the dermis of the epaxial region, not from migratory somitic cells in the hypaxial region. Furthermore, applying *sp7* fluorescent in situ hybridization chain reaction (HCR) to various ontogenetic stages, we confirmed that the somitic dorsal cleithrum is formed appositionally, following the initiation of the cleithrum ossification at the pharyngeal arch level (see Supplementary Note 2 and Supplementary Fig. 2h–p). In summary, our photoconversion and genetic lineage tracing show that the first four anterior somites contribute to the pectoral musculature and dorsal extremity of the cleithrum.

Trunk LPM contributes to the fin mesenchyme, lateral body wall, scapulocoracoid, and cleithrum

Next, to query the contribution of the trunk LPM to the pectoral girdle, we photoconverted the LPM at the prospective pectoral fin region (hereafter "fin-field LPM" as a subpopulation of the trunk LPM) of Kaede-injected embryos at the 10–12 somite stage (Fig. 3a, b). To label the fin-field LPM, we photoconverted the LPM at the level from the first to the third somite[32] (Fig. 3a, b). At 72 hpf, the photoconverted cells did not appear in skeletal muscles that arose from the anterior somites (Fig. 2), indicating that our photoconversion avoided ectopic labeling of adjacent somites (Fig. 3c–e). The labeled cells in the epidermis of the head and pectoral fin likely reflect ectopically labeled epidermal ectoderm (Fig. 3c, Supplementary Note 3). Labeled cells were also distributed in the endoskeletal disc, the scapulocoracoid ($n = 7/7$) (Fig. 3c; Supplementary Data 1), and additionally in the posterior margin of the cleithrum ($n = 5/7$) (Fig. 3f; Supplementary Data 1). These data indicate that LPM at the level of the prospective pectoral fin region contributes to the cleithrum.

To genetically corroborate the contribution of the LPM to the pectoral girdle, we labeled the LPM lineage using *drl:creERT2* transgenic zebrafish, in which the *draculin* (*drl*) regulatory region drives (Z)−4-hydroxytamoxifen (4-OHT)-inducible CreERT2 recombinase expression in the LPM[40] (see Methods, and Supplementary Table 1 for detailed strain information). Embryos obtained from crossing *drl:creERT2* and *hsp70l:Switch* reporter (in which EGFP is expressed upon Cre-mediated *loxP* recombination) were treated by 4-OHT from the shield stage to 24 hpf and subjected to heat shock at 72 hpf as previously described[30,41] (Supplementary Fig. 3). At 72 hpf, EGFP-labeled cells distributed in the cleithrohyoid muscle and the epithelium of the pharyngeal clefts (Supplementary Fig. 3a, c, d) are attributable to early-stage *drl* enhancer activity in the somitic lineage and endodermal epithelium of the pharynx, respectively[33,40]. Consistent with previous studies, EGFP-positive cells were observed in the pectoral fin and aortic arches[40,41] (Supplementary Fig. 3a, b, d). EGFP-labeled cells were enriched in the cartilage of the endoskeletal disc, scapulocoracoid, and cleithrum (Supplementary Fig. 3b, c). Additionally, in situ HCR confirmed that EGFP-positive cells in the cleithrum are osteoblasts expressing an osteoblast marker *sp7* (Fig. 3g, Supplementary Fig. 3c). Taken together, these results indicate that the region-specific photoconversion and genetic lineage labeling consistently identified the contribution of the LPM to the endoskeletal disc, scapulocoracoid, and cleithrum.

The LPM containing CPM-associated cells contributes to the cleithrum

To further confirm our finding using *drl:creERT2*-based LPM lineage labeling, we sought to refine the spatial photoconversion and genetic labeling into anterior LPM including prospective CPM-derived cells[30,31,40]. We photoconverted the ventrolateral head region at the post-otic level (hereafter "ventrolateral head region"), which contains the CPM, at the 10–12 somite stage (Fig. 4a). Immediately after photoconversion, we confirmed that the labeled ventrolateral head region contained the prospective CPM, epidermal ectoderm, and ventrolateral half of the post-otic placode (Fig. 4a, b; see also Supplementary Note 3). At 72 hpf, we found labeled cells in the epidermis in the head and pectoral fin, presumably due to ectopic photoconversion of the epidermal ectoderm (Fig. 4c–e). The entire vagus ganglia (derivatives of the epibranchial placode: $n = 8/8$) and the ventral portion of the posterior lateral line ganglion (a derivative of the lateral line placode: $n = 7/8$) were also labeled (Fig. 4d, e; Supplementary Data 1), which probably derived from the ectopically labeled ventrolateral half of the post-otic placode at the 10–12 somite stage (Fig. 4b). This result is consistent with the previously reported developmental fate of the post-otic placode[42,43]. Labeled cells were also found to delineate the bone matrix of the cleithrum without specific spatial distribution ($n = 7/8$) (Fig. 4f; Supplementary Data 1). In horizontal confocal sections, we found that the labeled cells surrounding the bone matrix of the cleithrum (Fig. 4g, h; white arrowheads) are contiguous with the mesenchymal cells at the posterior edge of the pericardial wall (Fig. 4g, h; black arrows) that itself originates from the LPM including *tbx1*-expressing presumptive CPM[31,41]. Overall, these results indicate that anterior LPM including CPM-associated cells (Fig. 4b) generates osteoblasts contributing to the cleithrum.

To corroborate the result of the anterior LPM and CPM photoconversion, we subsequently performed a genetic cell lineage tracing

https://doi.org/10.1038/s41467-024-50734-x

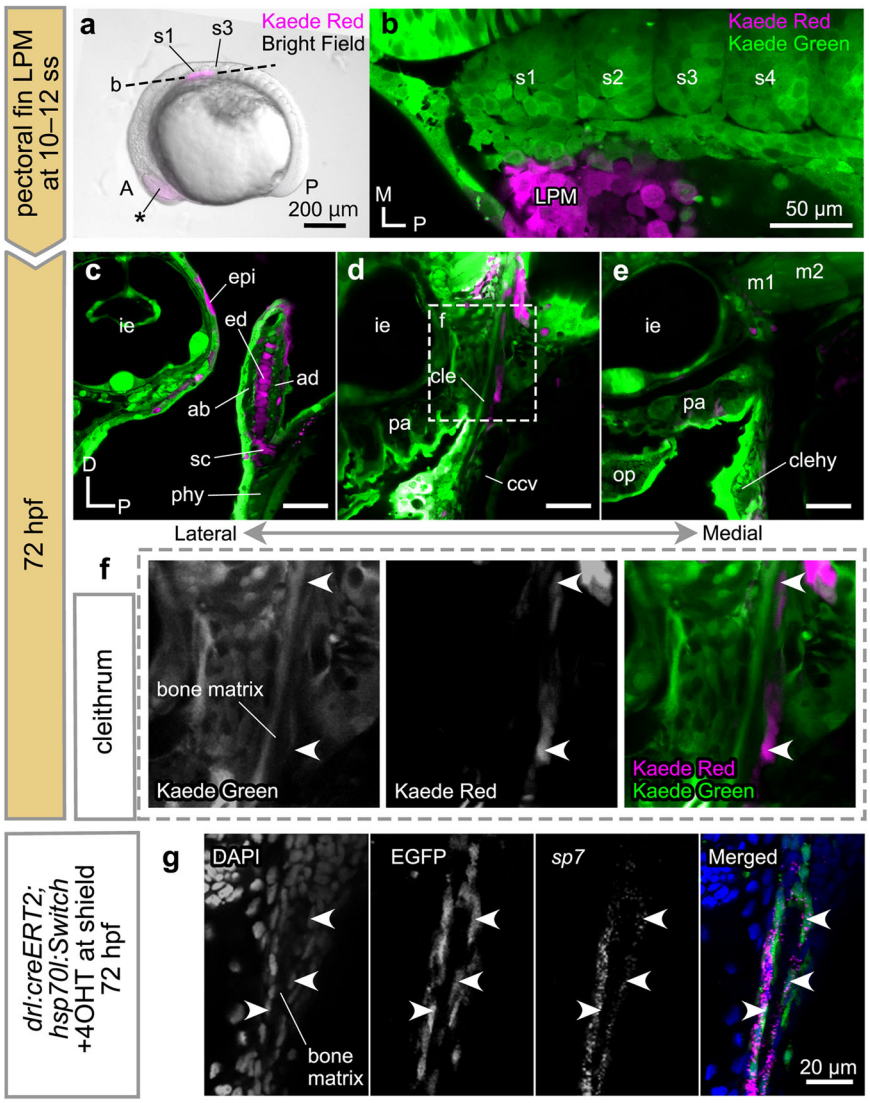

Fig. 3 | Contributions of the LPM to the pectoral girdle and fin skeleton. **a**, **b** Photoconversion of the LPM adjacent to somites 1–3 at the 10–12 somite stage (ss), viewed from the left lateral side (**a**) and in horizontal confocal section (**b**) ($n = 9$). Kaede-red is pseudo-colored in magenta. Asterisk in (**a**) shows the ectopically labeled optic vesicle. **c**–**e** At 72 hpf, parasagittal confocal sections obtained from mediolaterally different levels [lateral (**c**) to medial (**e**)] show that labeled cells are in the endoskeletal disc ($n = 7/7$), scapulocoracoid ($n = 7/7$), and (**f**) in the posterior half of the cleithrum ($n = 5/7$). **g** Contributions of the genetically labeled *drl:creERT2* lineage cells to the osteoblasts of the cleithrum. The obtained embryos were subjected to in situ HCR with *sp7* probe and DAPI staining. EGFP signal is raw fluorescence. Arrowheads in (**g**) point *drl:creERT2* lineage cells expressing *sp7* ($n = 3$).A anterior, ab abductor muscle, ad adductor muscle, ccv common cardinal vein, cle cleithrum, clehy cleithrohyoid muscle, D dorsal, ed endoskeletal disc, epi epidermis, ie inner ear, LPM lateral plate mesoderm, M medial, m1–2 myotomes 1–2, op operculum, P posterior, pa pharyngeal arches, phy posterior hypaxial muscle, s1–4 somites 1–4, sc scapulocoracoid. Scale bars: (**a**) 200 µm, (**b**–**e**) 50 µm, (**g**) 20 µm.

of *tbx1:creERT2;hsp70l:Switch* embryos (see Methods and Supplementary Table 1). The T-box transcription factor gene *Tbx1* shows evolutionarily conserved expression patterns in the pharyngeal mesoderm across chordates[44,45]. As such, the zebrafish *tbx1:creERT2* transgene indelibly labels cardiopharyngeal lineages, endoderm in the pharynx, and possibly trigeminal neural crest lineages in zebrafish embryos[30,41]. We treated embryos obtained from crossing *tbx1:creERT2* and *hsp70l:Switch* zebrafish with 4-OHT from the shield stage to 24 hpf and observed the distribution of EGFP-positive cells at 72 hpf as previously described[41] (Supplementary Fig. 4). Consistent with previous studies[30,41], EGFP-positive cells were observed among mesenchymal cells surrounding the inner ear and in pharyngeal musculature (Supplementary Fig. 4a–c). Additionally, labeled cells sparsely delineated the cleithrum bone matrix. In situ HCR confirmed that these cells are *sp7*-positive osteoblasts (Fig. 4i, Supplementary Fig. 4c), demonstrating *tbx1*-positive lineage contribution to the cleithrum. Labeled cells were also found in the epithelium of the pharyngeal clefts (Supplementary Fig. 4d), reflecting early *tbx1:creERT2* activity in the endodermal lineage, akin to *Tbx1* in mouse[30,46]. Taken together, the results of both photoconversion and genetic lineage tracing of the *tbx1:creERT2*-labeled lineage further support a contribution of the anterior LPM and presumptive CPM-associated cells to the zebrafish cleithrum (Fig. 4, Supplementary Fig. 4).

Branchial neural crest cells give rise to the pharyngeal mesenchyme and the anterior half of the cleithrum

Several elements of the tetrapod shoulder girdle integrate cells of different lineage origins[10–12,17–20]. In our LPM-focused experiments above, we noted highly mosaic lineage labeling in the cleithrum, indicating that the cleithrum might also integrate cells from additional lineage origins. The neural crest contributes to numerous features in the craniofacial skeleton as major evolutionary innovation in

https://doi.org/10.1038/s41467-024-50734-x

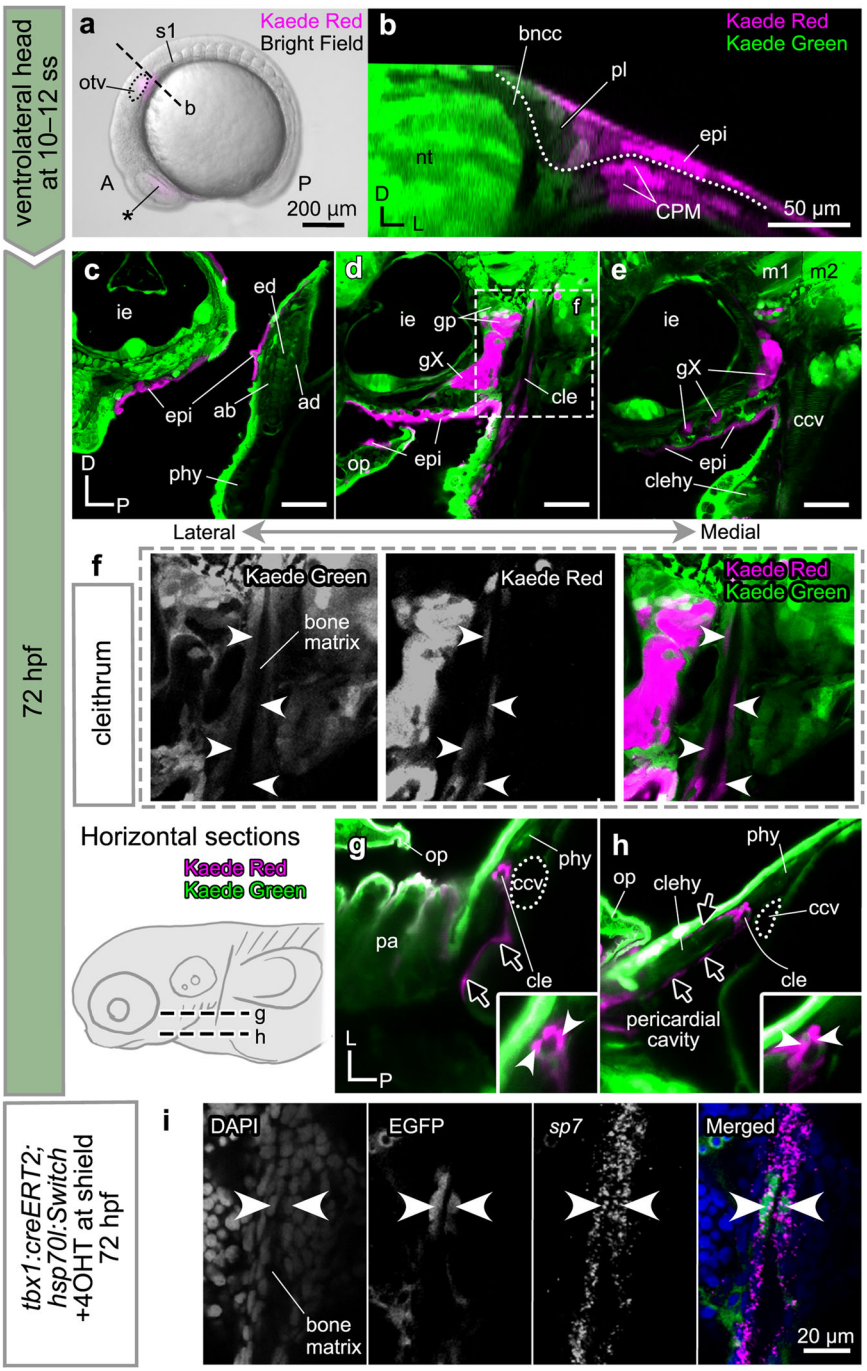

Fig. 4 | Contributions of CPM to the pectoral girdle and pericardium. **a**, **b** Photoconversion of the ventrolateral head region at the 10–12 somite stage (ss), viewed from lateral (**a**) and transverse confocal section (**b**) ($n = 10$). The photo-converted area (pseudo-colored in magenta) in (**b**) contains CPM. Dotted line in (**b**) depicts the interface between ectodermal epithelium and its underlying tissues. Asterisk in (**a**) shows the ectopically labeled optic vesicle. **c**–**e** At 72 hpf, parasagittal confocal sections at mediolaterally different levels [lateral (**c**) to medial (**e**)] show that labeled cells are in the ventral part of the posterior lateral line ganglion ($n = 7/8$), vagus nerve ganglia ($n = 8/8$), and (**f**) in the cleithrum ($n = 7/8$). **g**, **h** Horizontal confocal sections at different dorsoventral levels also show labeled cells in the cleithrum (white arrowheads) laterally adjacent to the common cardinal vein (outlined by a dotted line) ($n = 7/8$). Labeled cells are also observed in the pericardial wall (black arrows). **i** Contribution of the genetically labeled *tbx1:creERT2* lineage cells to osteoblasts of the cleithrum. The obtained embryos were subjected to in situ HCR with *sp7* probe and DAPI staining. EGFP signal is raw fluorescence. Arrowheads in (**i**) point *tbx1:creERT2* lineage cells expressing *sp7* ($n = 3$). A anterior, ab abductor muscle, ad adductor muscle, bncc branchial neural crest cells, ccv common cardinal vein, cle cleithrum, clehy cleithrohyoid muscle, CPM cardiopharyngeal mesoderm, D dorsal, ed endoskeletal disc, epi epidermis, gp posterior lateral line ganglion, gX vagus nerve ganglia, ie inner ear, L lateral, nt neural tube, op operculum, otv otic vesicle, P posterior, pa pharyngeal arches, phy posterior hypaxial muscle, pl placode, m1–2 myotomes 1–2, s1 first somite. Scale bars: (**a**) 200 µm, (**b**–**e**) 50 µm, (**i**) 20 µm.

vertebrates[47,48]. To date, a possible contribution of the neural crest to the cleithrum remains unclear. We therefore used photoconversion to revisit a potential cleithrum contribution of branchial neural crest cells, an evolutionarily conserved, posterior-most cranial neural crest stream in jawed vertebrates[49]. We first photoconverted the dorsomedial region of the embryonic head at the post-otic level (hereafter referred to as "dorsomedial head region" corresponding to a previously identified cardiac neural crest population[50]) in embryos ubiquitously expressing Kaede-green at the 10–12 somite stage (Fig. 5a). In situ HCR discerned a cell population positive for *foxd3*, a migrating neural crest cell marker[51], between the otic vesicle and first somite, confirming that the photoconverted dorsomedial head region includes the branchial neural crest cells (compare Fig. 5b with 5c). The adjacent otic vesicle, neural tube, epidermal ectoderm, and dorsomedial portion of the post-otic placode were also ectopically labeled (Fig. 5a, b, Supplementary Note 3). The lateral migrating frontier of the branchial neural crest stream at this stage does not reach beyond the placodal region (Fig. 5c) and does not enter into the ventrolateral head region (compare Fig. 4b with Fig. 5c), indicating that our photoconversions of the branchial neural crest cells (in the dorsomedial head region) and prospective CPM (in the ventrolateral region) were mutually exclusive.

At 72 hpf, Kaede-red labeled cells were found in the posterior wall of the inner ear, epidermis, and posterior lateral line ganglion (Fig. 5d–f), consistent with ectopic photoconversion of the otic vesicle, epidermal ectoderm, and dorsolateral half of the post-otic placode, respectively, using our laser-based approach (Fig. 5a, b). Nonetheless, the labeled mesenchymal cells around the vagus ganglia in the posterior pharyngeal arches match previously observed descendants of cranial neural crest cells[52], supporting our photoconversion efficacy (Fig. 5d–f). We also found that labeled cells delineate the anterior margin of the cleithrum ($n = 10/12$) (Fig. 5e, white arrowheads in Fig. 5g–i, Supplementary Data 1) and disseminate toward the labeled pharyngeal arch mesenchyme (black arrows in Fig. 5h). We also corroborated this result by conducting neural crest cell-specific photoconversion with *sox10:Kaede* embryos (see Supplementary Table 1). We altered the color of Kaede from green to red in the branchial neural crest region by UV illumination at the 12 somite stage (Supplementary Fig. 5a) and identified the photoconverted cells in the anterior margin of the cleithrum at 72 hpf (Supplementary Fig. 5b, c; white arrowheads. For our interpretations on other labeled tissues, see Supplementary Note 4.). All these observations persistently indicate a branchial neural crest cell contribution to the cleithrum in addition to our previously established somitic and LPM contribution.

To complementarily determine the neural crest distribution with genetic labeling, we first used *crestin:creERT2* with *ubi:Switch* as *loxP* reporter (GFP to mCherry change upon Cre activity; see Methods, and Supplementary Table 1). The *crestin* regulatory element deployed in this transgenic fish is selectively active in the premigratory and migratory neural crest cells after the somitogenesis stage[53,54]. We treated embryos with 4-OHT at the shield stage, imaged at 96 hpf, and observed mCherry-labeled cells in the opercle ($n = 4/6$), a pharyngeal arch derivative, and the cleithrum ($n = 2/6$; Supplementary Fig. 6a). Second, we obtained embryos from crossing *sox10:creERT2* and *actb2:Switch* reporter zebrafish (BFP to DsRed change upon Cre activity; see Methods, and Supplementary Table 1). The deployed zebrafish *sox10* promoter is active in premigratory/early migratory neural crest cells and the otic epithelium at 11–16 hpf and chondrocytes after 48 hpf[55–57]. To predominantly label migrating neural crest cells, we treated the embryos with 4-OHT from 11 – 24 hpf (Supplementary Fig. 6). At 72 hpf, DsRed-positive cells were found in mesenchymal cells in the operculum, pharyngeal arch mesenchyme, epithelium of the inner ear, and cleithrum (Supplementary Fig. 6b–e). In situ HCR confirmed that these DsRed-positive cells express *sp7* and reside in only the anterior half of the cleithrum (Fig. 5j, Supplementary Fig. 6d), consistent with the Kaede-based photoconversion result (Fig. 5g). Overall, the comprehensive and meticulous photoconversions and genetic labeling consistently demonstrated the contribution of cranial neural crest cells to the anterior half of the cleithrum at the posterior to the pharyngeal arch mesenchyme (Fig. 5g–j, Supplementary Figs. 5, 6).

Discussion

Our photoconversion and genetic-cell lineage tracing experiments here provide evidence that the zebrafish cleithrum develops as a composite bone of somitic cells, LPM-derived cells (the fin-field LPM and CPM-associated cells), and cranial neural crest cells, while the endoskeletal scapulocoracoid derives solely from the fin-field LPM (Fig. 6). The conflicting data of neural crest contribution from previous work[27] may be attributed to an activity difference between the mouse *Sox10* enhancer and the here deployed zebrafish *sox10* promoter[57], observations with which we further support using *crestin*-based genetic lineage labeling and targeted Kaede photoconversion (Fig. 5, Supplementary Figs. 5 and 6). Intriguingly, photoconverted fin-field LPM cells were found at the posterior margin of the cleithrum (Figs. 3 and 6) while branchial neural crest cells were found only at the anterior margin (Figs. 5 and 6). In contrast, *tbx1* lineage-labeled and generally CPM-associated LPM cells distributed throughout the cleithrum (Figs. 4 and 6). The spatially confined aggregation of the fin-field LPM and branchial neural crest cells in the cleithrum might result from the position of the cleithrum primordium which lies anteriorly to the pectoral fin bud and posteriorly to the pharynx[58]. Later, the cleithrum dorsally extends into the epaxial region and incorporates somitic cells, which become topographically available (Fig. 6b, Supplementary Fig. 2p). Intriguingly, the tetrapod endoskeletal scapula also arises from two distinct cell populations: the LPM and somitic/paraxial mesoderm[17,18,20]. Although the somitic contribution into the endoskeletal scapula could be a derived character in tetrapods due to the dorsal expansion of the scapula[2,20], similar position-dependent incorporation of the somitic cells may also be the case in the ontogenetic dorsal expansion of the zebrafish cleithrum (Fig. 6b). Formulating available evidence and our results, we postulate that the zebrafish larval cleithrum develops at the head/trunk interface by assembling topographically nearby cell populations at each ontogenetic stage, such as the head (CPM and cranial neural crest cells), trunk (fin-field LPM) mesenchyme, and later somitic cells (Fig. 6, Supplementary Fig. 7a). As previous research found indispensable genes for normal cleithrum formation[58–60], future genetic and molecular studies are warranted to functionally test these genes or identify the previously unknown molecular machinery that converges on the assembly of distinct embryonic cell populations into the cleithrum.

The head/trunk interface generates multiple structures, including the neck, that grants independent mobility to the skull from the pectoral girdle[61]. Neck musculoskeletal components have been reported to originate from a mixture of multiple embryonic cell populations in a variety of jawed vertebrates. In mice, neck musculatures, such as the trapezius, sternocleidomastoid, and infrahyoid muscles, contain connective tissues derived from a combination of cranial neural crest cells and LPM[11,12]. Moreover, the gill arch skeletons in cartilaginous fishes and amphibians and the laryngeal skeleton in amniotes develop as composites of cranial neural crest cells and CPM[62–65]. Likewise, the cleithrum develops between the pharyngeal arches and pectoral fin, deploying distinct cellular sources and, possibly, developmental genetic programs. Although the functional contributions or properties of these mixed embryonic origins in neck and shoulder girdle evolution remain limited, functional diversity of osteoblasts derived from several progenitor cell populations may be critical for development and evolution of the cleithrum, which was lost in amniotes during the posterior shift of the pectoral girdle due to the neck elongation (see below).

https://doi.org/10.1038/s41467-024-50734-x

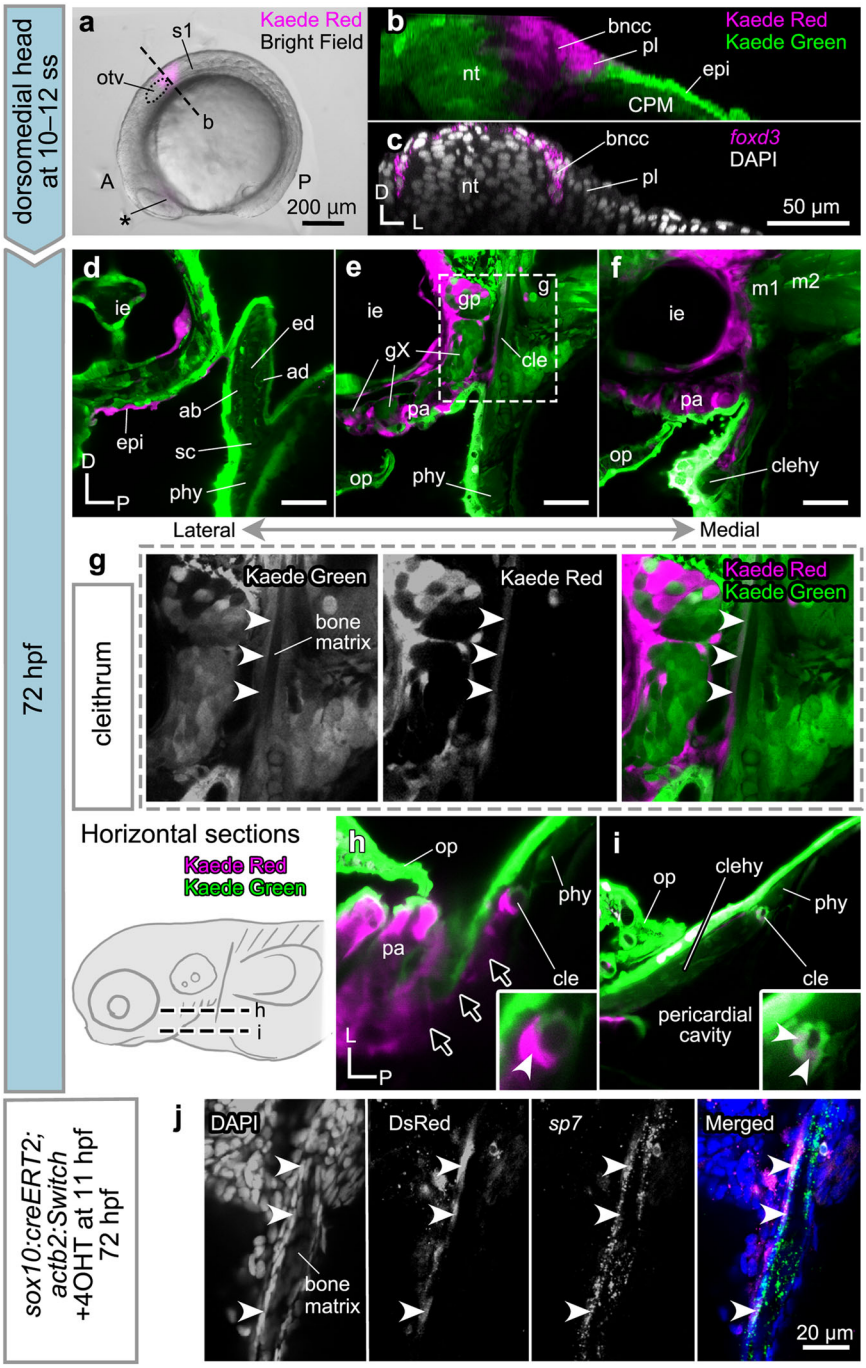

Fig. 5 | Contributions of cranial neural crest cells to the head and pectoral girdle. a, **b** Photoconversion of the dorsomedial head region at the 10–12 somite stage (ss) labels the branchial neural crest cells and adjacent neural tube, epidermis, and placode ($n = 15$). Asterisk in (**a**) points the faintly labeled optic vesicle. **c** *foxd3* in situ HCR image obtained from approximately at the same transverse level in (**b**). The lateral migratory frontier of branchial neural crest cells does not laterally exceed the level of the placode at this stage ($n = 3$). **d**–**f** At 72 hpf, parasagittal confocal sections at mediolaterally different levels [lateral (**d**) to medial (**f**)] show that labeled cells are in the dorsal part of the posterior lateral line ganglion (n = 11/12), mesenchymal cells in the pharyngeal arches ($n = 12/12$), and the anterior half of the cleithrum (**g**) ($n = 10/12$). **h**, **i** Horizontal confocal sections at different dorsoventral levels also show labeled cells in the cleithrum (white arrowheads). Labeled cells are continuously distributed from the pharyngeal arch mesenchyme to the cleithrum (black arrows) ($n = 10/12$). **j** Contribution of the genetically labeled *sox10:creERT2* lineage to osteoblasts of the cleithrum ($n = 3$). The obtained embryos were subjected to in situ HCR with *sp7* probe and DAPI staining, and then stained by DsRed immunofluorescence (see Methods). Arrowheads in (**j**) point *sox10:creERT2* lineage cells expressing *sp7*. A anterior, bncc branchial neural crest cells, cle cleithrum, clehy cleithrohyoid muscle, CPM cardiopharyngeal mesoderm, D dorsal, ed endoskeletal disc, epi epidermis, gp posterior lateral line ganglion, gX vagus nerve ganglia, ie inner ear, L lateral, nt neural tube, op operculum, otv otic vesicle, P posterior, pa pharyngeal arches, phy posterior hypaxial muscle, pl placode, m1–2 myotomes 1–2, s1 first somite, sc scapulocoracoid. Scale bars: (**a**) 200 µm, (**b**–**f**) 50 µm, (**j**) 20 µm.

https://doi.org/10.1038/s41467-024-50734-x

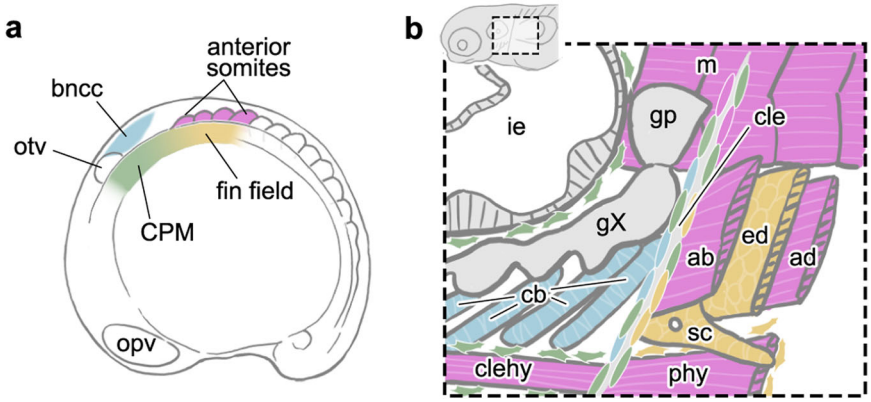

Fig. 6 | Embryonic origins and environment of the zebrafish pectoral girdle. **a** Four embryonic populations reside at the prospective pectoral girdle region at the 10–12 somite stage. They establish the embryonic head/trunk interface in the zebrafish embryo by the pharyngula stage. **b** Schematic drawing of the left pectoral region of a zebrafish larva. Based on its embryonic origin, each element follows the same color code as in (**a**): somites-derived, pink; fin-field LPM-derived, yellow; CPM-derived, green; branchial neural crest cell-derived, light blue. The anterior somites contribute to pectoral muscles and dorsal cleithrum. The branchial neural crest cells contribute to ceratobranchial cartilages and anterior ridge of the cleithrum. The CPM gives rise to mesenchymal cells surrounding the cleithrohyoid muscle and is mosaically distributed throughout the cleithrum. The fin-field LPM forms the posterior half of the cleithrum. The scapulocoracoid and endochondral disc originate exclusively from the fin-field LPM. The oval cells surrounding the bone matrix of the cleithrum represent osteoblasts. The distal portion of the pectoral fin elements and the posterior portion of the posterior hypaxial muscle is partially removed (cut surfaces are shaded). ab abductor muscle, ad adductor muscle, bncc branchial neural crest cells, cb ceratobranchial, cle cleithrum, CPM cardiopharyngeal mesoderm, ed endoskeletal disc, gp posterior lateral line ganglion, gX vagus ganglia, ie inner ear, m myotomes, opv optic vesicle, otv otic vesicle, phy posterior hypaxial muscle, sc scapulocoracoid.

The detailed analysis of the embryonic origins of the cleithrum and scapulocoracoid illuminates the intricate developmental mechanisms of the pectoral girdle in bony fishes. Several genetic mutant zebrafish with a complete loss of the pectoral fin and scapulocoracoid develop a completely or almost normal cleithrum (reviewed in ref. 28), suggestive of a certain degree of ontogenetic independency between the cleithrum and scapulocoracoid, at least during early pectoral girdle development. For example, *ikarus*-mutant zebrafish, which possess a stop codon mutation in *fgf24*, lack the scapulocoracoid with morphologically normal cleithrum[66]. *Fgf24* is expressed in the LPM and regulates mesenchyme migration and gene expressions indispensable for fin development. Consistent with our cell fate tracing demonstrating that the endoskeletal disc and scapulocoracoid arise exclusively from the LPM, *fgf24* mutation seems to chiefly affect the scapulocoracoid formation but not the adjacent cleithrum. The fin-field LPM contributes only to the posterior portion of the cleithrum and could be compensated by the CPM that also forms the posterior cleithrum (Fig. 6b). Concomitantly, the LPM could be responsible for the integration of cleithrum and scapulocoracoid developmental processes. A recent study identified that LPM cells differentiate to either osteoblasts in the cleithrum or chondrocytes in the scapulocoracoid depending on the intensity of hedgehog signaling[67]. This bipotency of LPM cells constructs the trade-off of development and evolution of the cleithrum and scapulocoracoid. Overall, the investigation of fish pectoral girdle origins explains a wide range of phenotypes that have been difficult to interpret by genetic knockout or genomics alone.

Multiple embryonic origins of the cleithrum provides novel insights into the origin of the pectoral girdle in fin-bearing gnathostomes. The head/trunk interface where the zebrafish cleithrum develops (Fig. 6) is embryologically defined as the distribution boundary between the head and trunk mesenchyme[68]. Importantly, anatomical structures around the interface (e.g., circumpharyngeal ridge, common cardinal vein, hypoglossal nerve, and hypoglossal cord) are highly preserved across all jawed vertebrates[68,69]; thus, the relative position of cleithrum with these anatomical structures serves as a means to infer the embryonic environment of the cleithrum in extinct and extant species. For instance, in Australian lungfish (*Neoceratodus*), an extant fin-bearing sarcopterygian, the topographical relationship among the circumpharyngeal ridge, common cardinal vein, pronephros, and cleithrum is comparable to that of zebrafish (see refs. 70,71. and compare with Fig. 1b). This conserved topographical relationship was likely established and fixed in the course of the stem-group gnathostomes[45,69,72]. Moreover, their tight topographical association even dates back to extinct osteostracans, jawless gnathostomes that possess early paired appendages and dermal pectoral girdle[73] (discussed in ref. 74). Thus, despite the anatomically derived characteristics of the teleost pectoral girdle among actinopterygians[6], the embryonic environment of the cleithrum identified in this study (Fig. 6) seems to be conserved across fishes bearing dermal pectoral girdles (also see Supplementary Discussion). We propose that, since its emergence, the pectoral girdle and appendage position has been confined to the posterior edge of the head and heart[72,75]. This ancestral developmental environment of the dermal pectoral girdle at the posterior edge of the head aligns with a recently proposed posterior pharyngeal origin of the pectoral girdle in placoderms[76]. Our findings also supports the dual embryonic origins of the pectoral complex (i.e., pectoral girdle and fin) as pharyngeal and trunk domains, bridging two mutually exclusive hypotheses on the evolutionary origin of pectoral appendages: the archipterygium hypothesis[77] and the fin-fold hypothesis[78,79] (see also discussion in ref. 10).

Early Synapsida and Sauropsida, such as *Edaphosaurus* (stem Synapsida) and Procolophonoidea (stem Sauropsida), retained the cleithrum even in their entirely terrestrial habitats[80,81]. However, along with increases in the cervical vertebral number and extension of the neck[82,83], their crown-groups, including all extant amniotes, completely lost the cleithrum[6,9]. In extant amniotes, the long neck integrates cells from a specialized trunk LPM region, namely the neck LPM[84], which is located between the head/trunk interface and forelimb bud (Supplementary Fig. 7b, c). The expansion of the neck LPM during development is critical for the posterior relocation of the heart and providing the mesenchymal environment for the diaphragm, which is a mammalian-specific structure[85–87] (Supplementary Fig. 7c). Given these developmental shifts, we hypothesize that the loss of the cleithrum in all extant amniotes may be attributed to the distant location of the

pectoral girdle from the branchial neural crest cell source (i.e., the head/trunk interface). Alternatively, the dispensability of the gill respiratory system supported by the cleithrum in terrestrial habitats might cause a loss of the genetic program for cleithrum formation. As a consequence, the cleithrum and associated dermal plates might have disappeared, and the functional neck originated in terrestrial vertebrates.

Recent studies have demonstrated that embryonic sources and morphological homology can be evolutionarily decoupled[20,21,62,88,89]. If this is the case in pectoral/shoulder girdle evolution, the embryonic sources for the cleithrum could vary in different fish species. Moreover, contrary to the above discussion, the cleithrum may not simply be a lost component in extant tetrapods; its developmental program may be maintained in the shoulder girdle even with its distinct embryonic environment[4]. Further studies of the cellular trajectories and molecular mechanisms underlying these cell differentiations in various cleithrum-bearing fishes are warranted to determine the possibility of decoupling of ontogenetic origins and homological traits over the course of pectoral/shoulder girdle evolution.

Methods

Zebrafish lines

Animal husbandry and experiments were carried out in accordance with the protocol approved by Institutional Animal Care and Use Committee (IACUC) of Rutgers University (protocol #: 201702646) and of the University of Colorado School of Medicine (protocol #: 00979). Adult zebrafish [*Danio rerio* (Hamilton, 1822)[90]] were kept at 28.5 °C on a 14 h light/10 h dark cycle. Wild-type zebrafish embryos were obtained from intercross of *AB (star-AB) line. Zebrafish transgenic lines used in this study include: *Tg(−6.3drl:creERT2, cryaa:Venus)*, *Tg(−3.2tbx1:creERT2, cryaa:Venus)*, *Tg(−1.5hsp70l:loxP-STOP-loxP-EGFP, cryaa:Venus)*, *Tg(−3.5ubi:loxP-GFP-loxP-mCherry)*, and *Tg(−4.9sox10:-creERT2;actb2:loxP-BFP-loxP-DsRed)*[30,40,56,91]. Additional transgenic lines are listed in the Supplementary Table 1. *sox10:creERT2* fish were identified by PCR (Forward primer: 5′-*TGCTGTTTCACTGGTTATGCGG* −3′ and reverse primer: 5′-*TTGCCCCTGTTTCACTATCCAG*−3′). Other transgenic fishes were screened by fluorescence markers—*cryaa:Venus, cryaa:YFP, ubi:Switch*, and *actb2:Switch*.

Staging

Since experimental conditions, such as photoconversion, overnight shipment, and heat shock may affect the developmental speed of zebrafish embryos, embryonic stages were determined based on external morphology not on absolute time, with reference to the staging table provided by ref. 37.

Photoconversion-based spatial lineage tracing

To prepare the DNA template for Kaede mRNA synthesis, the coding sequence of Kaede was subcloned from pME-Kaede vector into pCS2+ expression vector. Kaede mRNA was synthesized in vitro using mMESSAGE mMACHINE SP6 kit (AM1340, Invitrogen) following the manufacturer's instructions. To obtain zebrafish embryos with ubiquitous Kaede expression, Kaede mRNA diluted at 100 ng/μl in RNase-free water containing 0.005% phenol red (P0290-100ML, Sigma) was injected into the cytoplasm of wild-type embryos at one-cell stage using an MPPI-3 microinjector (ASI) under a stereomicroscope (S9E, Leica). Injected embryos were incubated in the embryo medium (10% Hank's with full strength calcium and magnesium: 13.7 mM NaCl, 0.54 mM KCl, 0.025 mM Na_2HPO_4, 0.044 mM KH_2PO_4, 1.3 mM $CaCl_2$, 1.0 mM $MgSO_4$, and 0.42 mM $NaHCO_3$). To photoconvert target embryonic regions at the 10–12 somite stage or 48 hpf, we embedded embryos into 0.7% low-gelling temperature agarose (50100, FMC BioProducts) in the embryo medium on a glass bottom dish (150680, Thermo Fisher Scientific) filled by phenol red-free L-15 medium (21083-027, Gibco). We then conducted photoconversion by illuminating 405 nm laser to the target regions for ~60 s on LSM510 Meta inverted confocal microscope (Zeiss). Labeled embryos were removed from the gel and incubated in six-well plates (657160, Greiner bio-one) filled with the embryo medium containing 0.003% 1-phenyl 2-thiourea (PTU; P7629, Sigma-Aldrich) at 28.5 °C until 72 hpf. Labeled embryos were anesthetized with 0.17 mg/ml ethyl 3-aminobenzoate methanesulfonate MS-222 (E10521-50G, Sigma-Aldrich), embedded in 0.7% agarose gel, and imaged alive with the confocal microscope. All labeled results are listed in Supplementary Data 1. For the consistency of the data, individuals with weak Kaede fluorescence or an excess amount of ectopic labeling (shown with asterisks in Supplementary Data 1) were omitted from the analysis (individuals highlighted in gray in Supplementary Data 1).

Photoconversions in *sox10:Kaede* embryos

Embryos obtained from *sox10:Kaede* adult fishes were photoconverted at the 10–12 somite stage as described above with the following modifications. To visualize tissues other than the neural crest cells during the photoconversion, *sox10:Kaede* embryos were raised in the embryo medium containing 2.5 μM BODIPY FL C5-Ceramide (D3521, Invitrogen) from immediately after fertilization to 10–12 somite stage.

Genetic lineage tracing

For heat-shock induction of *loxP* reporter cassettes driven by the *hsp70l* promoter and activation of CreERT2 in *drl:creERT2* and *tbx1:creERT2* lineages, we followed the previously reported procedures[41]. For CreERT2 activation in the *crestin:creERT2* and *sox10:creERT2* lineage, we added 5 μM 4-OHT to the embryo medium containing the dechorionated embryos from the shield stage to 24 hpf and 11 – 24 hpf, respectively. After the 4-OHT treatment, embryos were rinsed, raised to desired stages (72 or 96 hpf) in the embryo medium containing 0.003% PTU at 28.5 °C, and fixed by 4% paraformaldehyde (PFA) in phosphate-buffered saline (PBS) at 4 °C overnight.

In situ hybridization

Probe sets for HCR RNA fluorescence in situ hybridization were designed to be complementary to target transcripts and synthesized by Molecular Instruments (Supplementary Table 1). For the whole-mount in situ HCR, fixed embryos were washed with PBST (PBS containing 0.1% Tween 20 [P20370-1.0, RPI Research Products International]) at least three times. Subsequent procedures followed the manufacturer's instructions (MI-Protocol-RNAFISH-Zebrafish, Rev.#9)[92]. After the HCR, nuclei and actin were stained in PBST containing 5 μg/ml 4′,6-diamidino-2-phenylindole dihydrochloride (DAPI; D9542, Sigma-Aldrich) and Alexa Fluor 488 phalloidin (diluted in 1/100; A12379, Life Technologies), respectively, without light exposure at room temperature for two overnights.

Immunofluorescence

A duplexed in situ HCR and immunofluorescence has been performed as previously described[93] with minor modifications. Briefly, we omitted the methanol and acetone permeabilization steps before the whole mount HCR from the original protocol. Embryos after in situ HCR were washed with PBST and soaked in blocking solution [5% heat inactivated (56 °C, 30 min) sheep serum (S2263, Sigma-Aldrich) in PBST] at room temperature for 2 h. The blocking solution was replaced by a primary antibody solution [anti-mCherry rabbit polyclonal antibody (GTX128508, GeneTex) diluted in 1/200 in blocking solution]. Then, we incubated embryos with the primary antibody solution at 4 °C overnight. We washed the excess antibody solution by PBST and replaced the solution with a secondary antibody solution [anti-rabbit IgG Alexa Fluor 594 antibody (A11037, Invitrogen) diluted in 1/200]. Subsequently, we incubated embryos with a secondary antibody solution at 4 °C overnight. The excess secondary antibody solution was removed and embryos were washed with PBST and mounted in the 0.7% low-

gelling temperature agarose gel in PBST. Finally, mounted samples were subjected to a graded series of glycerol/PBST and transferred into 75% glycerol in PBST and imaged.

Imaging

Bright-field and fluorescence whole-mount images were photographed an upright microscope MZ16 (Leica) equipped with a digital camera MC170HD (Leica). Confocal sections were acquired by LSM510 Meta, LSM 800, and LSM 880 inverted confocal laser microscope equipped with a Plan-Apochromat 20x/0.8 M27, LD LCI Plan-Apochromat 25x/0.8 Imm Korr DIC M27, or C-Apochromat 40x/1.20 W Korr UV-VIS-IR M27 objective (Zeiss). The whole-mount and confocal images were processed by ImageJ (NIH) and ZEN 3.5 software (Zeiss), respectively. Volumetric 3D reconstructions from serial confocal images were performed by ZEN 3.5 software. Segmentation and 3D mesh generation were performed by Drishti 3.1[94] (https://github.com/nci/drishti) and rendered by Blender 2.80 (https://www.blender.org). Exported images in TIFF or PNG format were then assembled into figures in Adobe Photoshop (Adobe Systems). Three or more replicates were obtained for each imaging, unless otherwise described.

Reporting summary

Further information on research design is available in the Nature Portfolio Reporting Summary linked to this article.

Data availability

The data generated in photoconversion-based lineage tracing are available in the Supplementary Data 1. Abbreviations are listed within the file. Any imaging data generated in this study are available from the Figshare under the following (https://doi.org/10.6084/m9.figshare.26045854).

References

1. Goodrich, E. S. *Studies on the Structure and Development of Vertebrates* (Dover Publications Inc, 1930).
2. McGonnell, I. M. The evolution of the pectoral girdle. *J. Anat.* **199**, 189–194 (2001).
3. Gegenbaur, C. Clavicula und Cleithrum. *Morphol. Jahrb.* **23**, 1–20 (1895).
4. Matsuoka, T. et al. Neural crest origins of the neck and shoulder. *Nature* **436**, 347–355 (2005).
5. Gess, R. & Ahlberg, P. E. A tetrapod fauna from within the Devonian Antarctic circle. *Science* **360**, 1120–1124 (2018).
6. Jollie, M. *Chordate Morphology* (Reinhold, 1962).
7. Romer, A. S. & Parsons, T. S. *The Vertebrate Body* 6th edn, Vol. 656 (Thomson Learning, 1986).
8. Lyson, T. R. et al. Homology of the enigmatic nuchal bone reveals novel reorganization of the shoulder girdle in the evolution of the turtle shell. *Evol. Dev.* **15**, 317–325 (2013).
9. Romer, A. S. *Osteology of the Reptiles* Reprint edn (Krieger Publishing Company, 1997).
10. Nagashima, H. et al. Developmental origin of the clavicle, and its implications for the evolution of the neck and the paired appendages in vertebrates. *J. Anat.* **229**, 536–548 (2016).
11. Heude, E. et al. Unique morphogenetic signatures define mammalian neck muscles and associated connective tissues. *eLife* **7**, e40179 (2018).
12. Adachi, N., Bilio, M., Baldini, A. & Kelly, R. G. Cardiopharyngeal mesoderm origins of musculoskeletal and connective tissues in the mammalian pharynx. *Development* **147**, dev185256 (2020).
13. Nomaru, H. et al. Single cell multi-omic analysis identifies a *Tbx1*-dependent multilineage primed population in murine cardiopharyngeal mesoderm. *Nat. Commun.* **12**, 6645 (2021).
14. Prummel, K. D., Nieuwenhuize, S. & Mosimann, C. The lateral plate mesoderm. *Development* **147**, dev175059 (2020).
15. Wang, W. et al. A single-cell transcriptional roadmap for cardiopharyngeal fate diversification. *Nat. Cell Biol.* **21**, 674–686 (2019).
16. Lescroart, F., Dumas, C. E., Adachi, N. & Kelly, R. G. Emergence of heart and branchiomeric muscles in cardiopharyngeal mesoderm. *Exp. Cell Res.* **410**, 112931 (2022).
17. Shearman, R. M., Tulenko, F. J. & Burke, A. C. 3D reconstructions of quail-chick chimeras provide a new fate map of the avian scapula. *Dev. Biol.* **355**, 1–11 (2011).
18. Valasek, P. et al. Somitic origin of the medial border of the mammalian scapula and its homology to the avian scapula blade. *J. Anat.* **216**, 482–488 (2010).
19. Durland, J. L., Sferlazzo, M., Logan, M. & Burke, A. C. Visualizing the lateral somitic frontier in the Prx1Cre transgenic mouse. *J. Anat.* **212**, 590–602 (2008).
20. Piekarski, N. & Olsson, L. A somitic contribution to the pectoral girdle in the axolotl revealed by long-term fate mapping. *Evol. Dev.* **13**, 47–57 (2011).
21. Fabian, P. & Crump, J. G. Reassessing the embryonic origin and potential of craniofacial ectomesenchyme. *Semin. Cell Dev. Biol.* **138**, 45–53 (2023).
22. Etchevers, H. C., Dupin, E. & Le Douarin, N. M. The diverse neural crest: from embryology to human pathology. *Development* **146**, dev169821 (2019).
23. Epperlein, H. H., Khattak, S., Knapp, D., Tanaka, E. M. & Malashichev, Y. B. Neural crest does not contribute to the neck and shoulder in the axolotl (*Ambystoma mexicanum*). *PLoS One* **7**, e52244 (2012).
24. McGonnell, I. M., McKay, I. J. & Graham, A. A population of caudally migrating cranial neural crest cells: functional and evolutionary implications. *Dev. Biol.* **236**, 354–363 (2001).
25. Aoto, K. et al. *Mef2c-F10N* enhancer driven β-galactosidase (LacZ) and Cre recombinase mice facilitate analyses of gene function and lineage fate in neural crest cells. *Dev. Biol.* **402**, 3–16 (2015).
26. Masselink, W. et al. A somitic contribution to the apical ectodermal ridge is essential for fin formation. *Nature* **535**, 542–546 (2016).
27. Kague, E. et al. Skeletogenic fate of zebrafish cranial and trunk neural crest. *PLoS ONE* **7**, e47394 (2012).
28. Mercader, N. Early steps of paired fin development in zebrafish compared with tetrapod limb development. *Dev. Growth Differ.* **49**, 421–437 (2007).
29. Mongera, A. et al. Genetic lineage labeling in zebrafish uncovers novel neural crest contributions to the head, including gill pillar cells. *Development* **140**, 916–925 (2013).
30. Felker, A. et al. Continuous addition of progenitors forms the cardiac ventricle in zebrafish. *Nat. Commun.* **9**, 2001 (2018).
31. Prummel, K. D. et al. Hand2 delineates mesothelium progenitors and is reactivated in mesothelioma. *Nat. Commun.* **13**, 1677 (2022).
32. Mao, Q., Stinnett, H. K. & Ho, R. K. Asymmetric cell convergence-driven zebrafish fin bud initiation and pre-pattern requires Tbx5a control of a mesenchymal Fgf signal. *Development* **142**, 4329–4339 (2015).
33. Sagarin, K. A., Redgrave, A. C., Mosimann, C., Burke, A. C. & Devoto, S. H. Anterior trunk muscle shows mix of axial and appendicular developmental patterns. *Dev. Dyn.* **248**, 961–968 (2019).
34. Minchin, J. E. N. et al. Oesophageal and sternohyal muscle fibres are novel Pax3-dependent migratory somite derivatives essential for ingestion. *Development* **140**, 2972–2984 (2013).
35. Talbot, J. C. et al. Muscle precursor cell movements in zebrafish are dynamic and require Six family genes. *Development* **146**, dev171421 (2019).
36. Hatta, K., Tsujii, H. & Omura, T. Cell tracking using a photoconvertible fluorescent protein. *Nat. Protoc.* **1**, 960–967 (2006).
37. Kimmel, C. B., Ballard, W. W., Kimmel, S. R., Ullmann, B. & Schilling, T. F. Stages of embryonic development of the zebrafish. *Dev. Dyn.* **203**, 253–310 (1995).

38. Lee, R. T. H., Knapik, E. W., Thiery, J. P. & Carney, T. J. An exclusively mesodermal origin of fin mesenchyme demonstrates that zebrafish trunk neural crest does not generate ectomesenchyme. *Development* **140**, 2923–2932 (2013).
39. Wardle, F. C. & Papaioannou, V. E. Teasing out T-box targets in early mesoderm. *Curr. Opin. Genet. Dev.* **18**, 418–425 (2008).
40. Mosimann, C. et al. Chamber identity programs drive early functional partitioning of the heart. *Nat. Commun.* **6**, 8146 (2015).
41. Lalonde, R. L. et al. Heterogeneity and genomic loci of ubiquitous transgenic Cre reporter lines in zebrafish. *Dev. Dyn.* **251**, 1754–1773 (2022).
42. Šestak, M. S., Božičević, V., Bakarić, R., Dunjko, V. & Domazet-Lošo, T. Phylostratigraphic profiles reveal a deep evolutionary history of the vertebrate head sensory systems. *Front. Zool.* **10**, 18 (2013).
43. McCarroll, M. N. et al. Graded levels of Pax2a and Pax8 regulate cell differentiation during sensory placode formation. *Development* **139**, 2740–2750 (2012).
44. Onimaru, K., Shoguchi, E., Kuratani, S. & Tanaka, M. Development and evolution of the lateral plate mesoderm: Comparative analysis of amphioxus and lamprey with implications for the acquisition of paired fins. *Dev. Biol.* **359**, 124–136 (2011).
45. Adachi, N., Pascual-Anaya, J., Hirai, T., Higuchi, S. & Kuratani, S. Development of hypobranchial muscles with special reference to the evolution of the vertebrate neck. *Zool. Lett.* **4**, 5 (2018).
46. Arnold, J. S. et al. Inactivation of *Tbx1* in the pharyngeal endoderm results in 22q11DS malformations. *Development* **133**, 977–987 (2006).
47. Kuratani, S. & Ahlberg, P. E. Evolution of the vertebrate neurocranium: problems of the premandibular domain and the origin of the trabecula. *Zool. Lett.* **4**, 1 (2018).
48. Gans, C. & Northcutt, R. G. Neural crest and the origin of vertebrates: a new head. *Science* **220**, 268–273 (1983).
49. Stundl, J. et al. Migratory patterns and evolutionary plasticity of cranial neural crest cells in ray-finned fishes. *Dev. Biol.* **467**, 14–29 (2020).
50. Sato, M. & Yost, H. J. Cardiac neural crest contributes to cardiomyogenesis in zebrafish. *Dev. Biol.* **257**, 127–139 (2003).
51. Montero-Balaguer, M. et al. The mother superior mutation ablates *foxd3* activity in neural crest progenitor cells and depletes neural crest derivatives in zebrafish. *Dev. Dyn.* **235**, 3199–3212 (2006).
52. Abrial, M. et al. TGF-β signaling is necessary and sufficient for pharyngeal arch artery angioblast formation. *Cell Rep.* **20**, 973–983 (2017).
53. Kaufman, C. K. et al. A zebrafish melanoma model reveals emergence of neural crest identity during melanoma initiation. *Science* **351**, aad2197 (2016).
54. Luo, R., An, M., Arduini, B. L. & Henion, P. D. Specific pan-neural crest expression of zebrafish *crestin* throughout embryonic development. *Dev. Dyn.* **220**, 169–174 (2001).
55. Dutton, J. R. et al. An evolutionarily conserved intronic region controls the spatiotemporal expression of the transcription factor Sox10. *BMC Dev. Biol.* **8**, 105 (2008).
56. Giovannone, D. et al. Programmed conversion of hypertrophic chondrocytes into osteoblasts and marrow adipocytes within zebrafish bones. *eLife* **8**, e42736 (2019).
57. Carney, T. J. et al. A direct role for Sox10 in specification of neural crest-derived sensory neurons. *Development* **133**, 4619–4630 (2006).
58. Heude, É., Shaikho, S. & Ekker, M. The *dlx5a/dlx6a* genes play essential roles in the early development of zebrafish median fin and pectoral structures. *PLoS ONE* **9**, e98505 (2014).
59. Grandel, H. et al. Retinoic acid signalling in the zebrafish embryo is necessary during pre-segmentation stages to pattern the anterior-posterior axis of the CNS and to induce a pectoral fin bud. *Development* **129**, 2851–2865 (2002).
60. Neumann, C. J., Grandel, H., Gaffield, W., Schulte-Merker, S. & Nüsslein-Volhard, C. Transient establishment of anteroposterior polarity in the zebrafish pectoral fin bud in the absence of *sonic hedgehog* activity. *Development* **126**, 4817–4826 (1999).
61. Trinajstic, K. et al. Fossil musculature of the most primitive jawed vertebrates. *Science* **341**, 160–164 (2013).
62. Sleight, V. A. & Gillis, J. A. Embryonic origin and serial homology of gill arches and paired fins in the skate, *Leucoraja erinacea*. *eLife* **9**, e60635 (2020).
63. Evans, D. J. & Noden, D. M. Spatial relations between avian craniofacial neural crest and paraxial mesoderm cells. *Dev. Dyn.* **235**, 1310–1325 (2006).
64. Tabler, J. M. et al. Cilia-mediated Hedgehog signaling controls form and function in the mammalian larynx. *eLife* **6**, e19153 (2017).
65. Sefton, E. M., Piekarski, N. & Hanken, J. Dual embryonic origin and patterning of the pharyngeal skeleton in the axolotl (*Ambystoma mexicanum*). *Evol. Dev.* **17**, 175–184 (2015).
66. Fischer, S., Draper, B. W. & Neumann, C. J. The zebrafish *fgf24* mutant identifies an additional level of Fgf signaling involved in vertebrate forelimb initiation. *Development* **130**, 3515–3524 (2003).
67. Wei, J. et al. Distinct ossification trade-offs illuminate the shoulder girdle reconfiguration at the water-to-land transition. *bioRxiv* https://doi.org/10.1101/2023.07.17.547998 (2023).
68. Kuratani, S. Spatial distribution of postotic crest cells defines the head/trunk interface of the vertebrate body: embryological interpretation of peripheral nerve morphology and evolution of the vertebrate head. *Anat. Embryol.* **195**, 1–13 (1997).
69. Higashiyama, H. et al. On the vagal cardiac nerves, with special reference to the early evolution of the head-trunk interface. *J. Morphol.* **277**, 1146–1158 (2016).
70. Hirasawa, T. et al. Development of the pectoral lobed fin in the Australian lungfish *Neoceratodus forsteri*. *Front. Ecol. Evol.* https://doi.org/10.3389/fevo.2021.679633 (2021).
71. Greil, A. Entwickelungsgeschichte des Kopfes und des Blutgefäßsystems von *Ceratodus forsteri*. II. Die epigenetischen Erwerbungen während der Stadien 39-48. *Denkschriften der Medicinisch-Naturwissenschaftlichen Ges. zu Jena.* **4**, 935–1492 (1913).
72. Trinajstic, K. et al. Exceptional preservation of organs in Devonian placoderms from the Gogo lagerstätte. *Science* **377**, 1311–1314 (2022).
73. Janvier, P., Percy, L. R. & Potter, I. C. The arrangement of the heart chambers and associated blood vessels in the Devonian osteostracan *Norselaspis glacialis*. A reinterpretation based on recent studies of the circulatory system in lampreys. *J. Zool.* **223**, 567–576 (1991).
74. Adachi, N., Robinson, M., Goolsbee, A. & Shubin, N. H. Regulatory evolution of *Tbx5* and the origin of paired appendages. *Proc. Natl Acad. Sci. USA* **113**, 10115–10120 (2016).
75. Janvier, P. *Early Vertebrates* (Oxford University Press, 1996).
76. Brazeau, M. D. et al. Fossil evidence for a pharyngeal origin of the vertebrate pectoral girdle. *Nature* **623**, 550–554 (2023).
77. Gegenbaur, C. Zur Morphologie der Gliedmaassen der Wirbeltiere. *Morpho. Jahrb.* **2**, 396–420 (1876).
78. Thacher, J. K. Median and paired fins: a contribution to the history of vertebrate limbs. *Trans. Conn. Acad. Arts Sci.* **3**, 281–308 (1877).
79. Balfour, F. M. On the development of the skeleton of the paired fins of Elasmobranchii, considered in relation to its bearings on the nature of the limbs of the Vertebrata. *Proc. Zool. Soc. Lond.* **49**, 656–670 (1881).
80. Williston, S. W. *The Osteology of the Reptiles,* reprint edn (Krieger Publishing Company, 1925).
81. MacDougall, M. J. & Modesto, S. P. & Botha-Brink, J. The postcranial skeleton of the Early Triassic parareptile *Sauropareion anoplus*, with a discussion of possible life history. *Acta Palaeontol. Polonica* **58**, 737–749 (2013).

82. Hirasawa, T. & Kuratani, S. A new scenario of the evolutionary derivation of the mammalian diaphragm from shoulder muscles. *J. Anat.* **222**, 504–517 (2013).
83. Müller, J. et al. Homeotic effects, somitogenesis and the evolution of vertebral numbers in recent and fossil amniotes. *Proc. Natl Acad. Sci. USA* **107**, 2118–2123 (2010).
84. Lours, C. & Dietrich, S. The dissociation of the Fgf-feedback loop controls the limbless state of the neck. *Development* **132**, 5553–5564 (2005).
85. Hirasawa, T., Fujimoto, S. & Kuratani, S. Expansion of the neck reconstituted the shoulder-diaphragm in amniote evolution. *Dev., Growth Differ.* **58**, 143–153 (2016).
86. Sefton, E. M., Gallardo, M. & Kardon, G. Developmental origin and morphogenesis of the diaphragm, an essential mammalian muscle. *Dev. Biol.* **440**, 64–73 (2018).
87. Sefton, E. M. et al. Fibroblast-derived *Hgf* controls recruitment and expansion of muscle during morphogenesis of the mammalian diaphragm. *eLife* **11**, e74592 (2022).
88. Schneider, R. A. Neural crest can form cartilages normally derived from mesoderm during development of the avian head skeleton. *Dev. Biol.* **208**, 441–455 (1999).
89. Teng, C. S., Cavin, L., Maxson, R. E. J., Sánchez-Villagra, M. R. & Crump, J. G. Resolving homology in the face of shifting germ layer origins: Lessons from a major skull vault boundary. *eLife* **8**, e52814 (2019).
90. Hamilton, F. *An Account of the Fishes Found in the River Ganges and its Branches* Vol. 415 (Isha Books, 1822).
91. Mosimann, C. et al. Ubiquitous transgene expression and cre-based recombination driven by the *ubiquitin* promoter in zebrafish. *Development* **138**, 169–177 (2011).
92. Choi, H. M. T. et al. Third-generation in situ hybridization chain reaction: multiplexed, quantitative, sensitive, versatile, robust. *Development* **145**, dev165753 (2018).
93. Ibarra-García-Padilla, R., Howard, A. G. A., Singleton, E. W. & Uribe, R. A. A protocol for whole-mount immuno-coupled hybridization chain reaction (WICHCR) in zebrafish embryos and larvae. *STAR Protoc.* **2**, 100709 (2021).
94. Hu, Y., Limaye, A. & Lu, J. Three-dimensional segmentation of computed tomography data using *drishti paint*: new tools and developments. *R. Soc. Open Sci.* **7**, 201033 (2020).
95. Hildebrand, D. G. C. et al. Whole-brain serial-section electron microscopy in larval zebrafish. *Nature* **545**, 345–349 (2017).

Acknowledgements

This research was supported by the National Science Foundation under Grant IOS 2210072 and the Institutional support provided by the Rutgers University School of Arts and Sciences and the Human Genetics Institute of New Jersey to T.N.; the Children's Hospital Colorado Foundation and the Helen and Arthur E. Johnson Chair for the Cardiac Research Director, Additional Ventures SVRF2021-1048003, and the University of Colorado School of Medicine to C.M.; NIH/NHLBI 1K99HL168148-01 to R.L.L. We thank Gage Crump and Claire Arata for providing *sox10:-creERT2;actb2:Switch* embryos; Eric C. Liao, Eileen L. Dalessandro, and Lisa Tsay for providing *sox10:Kaede* fish; Charles K. Kaufman for providing adult *crestin:creERT2* and pioneering work on cleithrum labeling; Hannah Cohen, Kathleen Flaherty, and all other lab members in Nakamura lab for maintaining zebrafish colonies in the fish facilities at Rutgers University; Christine Archer, Ainsley Gilbard, and Olivia Gomez for excellent zebrafish husbandry support at CU Anschutz; Hiroyasu Kamei and his lab members for zebrafish husbandry support at Kanazawa University; Satoru Okuda for allowing us to access their laboratory equipment; and Kazutaka Hosoda and Oki Hayasaka for helpful discussion.

Author contributions

S.K. and T.N. conceived the project and designed the experiments. S.K. performed molecular, lineage tracing, and histological experiments. T.N. performed lineage tracing experiments using the *sox10:Kaede* and *tbx6:cre;ubi:Switch*. R.L.L., T.A.M., and C.M. conducted genetic lineage tracing experiments with *drl:creERT2*, *tbx1:creERT2*, and *crestin:creERT2* zebrafish. S.K., R.L.L., C.M., and T.N. wrote the manuscript.

Competing interests

The authors declare no competing interests.

Additional information

Supplementary information The online version contains supplementary material available at https://doi.org/10.1038/s41467-024-50734-x.

Correspondence and requests for materials should be addressed to Shunya Kuroda or Tetsuya Nakamura.

Peer review information *Nature Communications* thanks Joost Woltering and the other, anonymous, reviewers for their contribution to the peer review of this work. A peer review file is available.